JOURNAL OF PETROLOGY | VOLUME 46 | NUMBER 8 | PAGES 1565–1583 | 2005 | doi:10.1093/petrology/egi026

On the Use of Changes in Dihedral Angle to Decode Late-stage Textural Evolution in Cumulates

MARIAN B. HOLNESS[1]*, MICHAEL J. CHEADLE[2] AND DAN McKENZIE[1]

[1]DEPARTMENT OF EARTH SCIENCES, UNIVERSITY OF CAMBRIDGE, DOWNING STREET, CAMBRIDGE CB2 3EQ, UK
[2]DEPARTMENT OF GEOLOGY AND GEOPHYSICS, UNIVERSITY OF WYOMING, 1000 UNIVERSITY AVENUE, LARAMIE, WY 82070, USA

RECEIVED AUGUST 5, 2004; ACCEPTED FEBRUARY 14, 2005
ADVANCE ACCESS PUBLICATION MARCH 18, 2005

The melt-filled pore structure in the final stages of solidification of cumulates must lie somewhere between the two end-members of impingement (in which pore topology is controlled entirely by the juxtaposition of growth faces of adjacent grains) and textural equilibrium (in which pore topology is controlled by the minimization of internal energies). The exact position between these two end-members is controlled by the relative rates of crystal growth and textural equilibration. For samples in which growth has stopped, or is very slow, textural equilibrium will prevail. A close examination of dihedral angles in natural examples demonstrates that these two end-member textures can be distinguished. The impingement end-member results in a population of apparent solid–melt dihedral angles with a median of ~60° and a standard deviation of ~25–30°, whereas the texturally equilibrated end-member population has a median of ~28° and a standard deviation of ~14°. For the specific case of cumulates in the Rum Layered Intrusion, residual porosity in troctolitic cumulates was close to the impingement end-member, whereas that in peridotites was close to melt-bearing textural equilibrium. Suites of glass-bearing samples from small, or frequently disturbed, magma systems show modification of initial impingement textures. These modifications may be a consequence of textural equilibration or of diffusion-limited growth during quenching. Distinction can be made between these two processes by a consideration of grain shape. The geometry of interstitial phases in suites of fully solidified cumulates from the Rum Layered Intrusion shows variable approach to sub-solidus textural equilibrium from an initial state inherited by pseudmorphing of the last melt. Textural equilibration at pore corners occurs as a continuous process, with a gradual movement of the entire dihedral angle population towards the equilibrium final state. If the initial, pseudomorphed state is one of disequilibrium (i.e. a melt-present impingement texture) this change is accompanied by a reduction in the spread of the population. If it is one of equilibrium, the change is accompanied by an initial increase in the spread of the population, followed by a decrease. These observations demonstrate that previously published models of dihedral angle change involving the instantaneous establishment of the equilibrium angle in the immediate vicinity of the pore corner are incorrect.

KEY WORDS: *cumulate; dihedral angle; textural evolution; Rum intrusion; Kula; Santorini*

INTRODUCTION

The residence of magma in crustal chambers plays a vital part in the final composition of erupted lavas. This is because separation of crystals and residual liquid during cooling in the chamber results in chemical fractionation. A full understanding of the way magma chambers operate thus depends on a good understanding of the formation and development of crystal mushes forming at the thermal boundary layers of the chamber. Field observations of dissected basic and ultrabasic intrusions demonstrate that the most important of these boundary layers is the chamber floor (Hunter, 1996).

Cumulate development is a problem generally approached via a detailed study of textural relationships between minerals. Wager *et al.* (1960) developed a

*Corresponding author. E-mail: marian@esc.cam.ac.uk

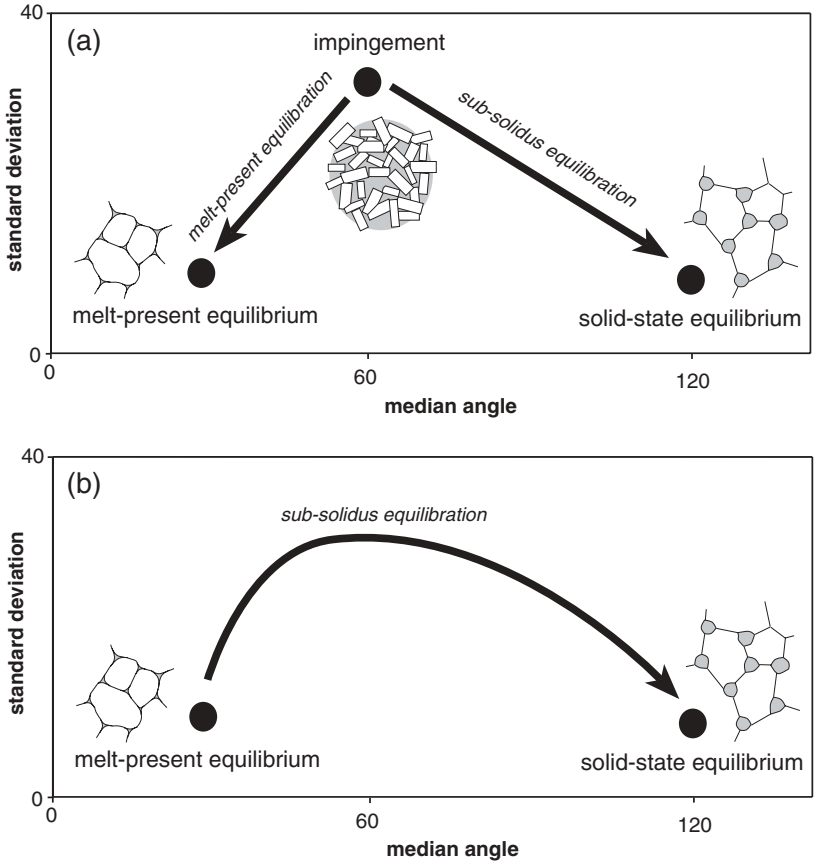

Fig. 1. Schematic diagrams showing the different end-point dihedral angle populations and the expected changes in these populations in response to textural maturation. (a) A melt-bearing crystal mush in which grain shape is dominated by growth processes will have a solid–solid–melt dihedral angle population with a median of 60° and a high standard deviation. This is termed an impingement texture. If the mush were then to equilibrate, the melt–solid–solid dihedral angle population will move towards one of low median and low standard deviation. For mushes containing a single solid phase with no anisotropy of interfacial energy, the standard deviation of this population would be zero. If the mush were to solidify, with pseudomorphing of the original melt-filled pore structure by a solid phase, then the dihedral angle population moves towards that of solid-state equilibrium, for which the dihedral angle population has a mean value of ~120° and a low standard deviation. (b) For the case in which an original, texturally equilibrated, melt-filled porosity is pseudomorphed by a solid phase, the transition from the inherited dihedral angle population towards solid-state equilibrium will involve an initial increase in standard deviation as a result of variable equilibration rates within the system. Schematic diagrams showing the different topology of the interstitial phase (either melt or solid) are based on the assumption of complete textural equilibration, whereas in fact the dihedral angle population will arrive at the new position before the surface curvature can completely adjust.

descriptive model based on the distinction between primary cumulus grains and post-accumulation interstitial grains that formed directly from the intergranular liquid phase. There has been much discussion and development of this early paradigm (e.g. McBirney & Hunter, 1995), with some workers pointing out that cumulus material may have grown *in situ* (e.g. Campbell, 1978; Maaløe, 1987), and not in the bulk of the chamber (or at the chamber roof) with the subsequent gravity-driven settling on the floor implicit in the model of Wager *et al.* (1960) (e.g. Irvine, 1987; Tepley & Davidson, 2003). Furthermore, Hunter (1987) suggested that some grains with apparent cumulus character may have begun life as post-cumulus interstitial material, with significant later change in shape driven by the reduction of interfacial energies.

Irrespective of the precise location of growth of cumulus crystals, it is clear that at any time the melt-filled pore structure in a crystal mush must lie somewhere between two possible end-members (Fig. 1). One of these end-members is controlled by the growth and impingement of crystals. In such a mush, the melt-filled pores are bounded by growth faces of the adjacent crystals, with a shape controlled by the relative orientation and shape of the impinging grains. The other is one in which pore shape is controlled by the minimization of interfacial energies; that is, it is texturally equilibrated.

This concept is the poly-crystalline analogue of the two possible end-member types of crystal shape for a grain suspended in an isotropic medium: one dominated by growth kinetics [which commonly results in planar faces, although these may be unstable relative to cellular

forms (Tiller, 1991; Jamtveit & Andersen, 1992)]; and the other dominated by the minimization of interfacial energy. The latter is a sphere for a perfectly isotropic substance, but anisotropy of interfacial energies results in the stabilization of flat facets, which may coexist with curved surfaces or cover the entire surface area of the grain (Herring, 1951*a*). Because the growth form is a function of growth rate and mechanism, and the composition of the growth medium (Donaldson, 1976; Swanson & Fenn, 1986; Didymus *et al.*, 1993; Faure *et al.*, 2003), in general the growth form will not be the same as the equilibrium form.

Because crystal shapes controlled by growth kinetics may be distinguishable from equilibrium shapes, crystal shape can be used to distinguish between an impingement texture and an equilibrated texture. Such a distinction is based on the understanding that planar faces may be a result of growth, and do not necessarily appear in the equilibrium form. With the relatively well-known extent of anisotropy of silicate minerals (e.g. Kretz, 1966; Laporte, 1994; Lupulescu & Watson, 1999), one would expect the transition from an impingement texture towards equilibrium to involve some rounding of the crystals [although some facets will remain if they are present in the equilibrium form (Herring, 1951*a*; Cahn & Handwerker, 1993)].

The actual topology of the melt in the last stages of solidification, whether it is controlled by impingement or textural equilibrium, plays an important role in cumulate development. This is because the physical characteristics of a mush with an impingement texture are very different from those with a fully equilibrated fluid-bearing texture (at least for systems with low anisotropy, in which texturally equilibrated grains are significantly rounded), with significant differences in permeability–porosity relationships at low melt fractions. The percolation threshold of a mush with an impingement texture is believed to be in the region of 8–11 vol. % (Cheadle *et al.*, 2004), rather than the infinitesimally low percolation threshold expected for fully equilibrated (isotropic) geologically relevant mushes, or thresholds in the region of 0·05–0·3 vol. % for fully equilibrated, realistically anisotropic, systems (Brenan, 1993; Minarik & Watson, 1995; Maumus *et al.*, 2004).

Under conditions where growth forms dominate, the angle subtended at pore corners in a crystal mush (the apparent dihedral angle) will have a median value of 60° if the crystals impinge at random orientations (as the sum of internal angles in a triangle is 180°) (Elliott *et al.*, 1997). The population of angles will have a high standard deviation about the mean (Elliott *et al.*, 1997; Fig. 1). For a texturally equilibrated mush, the population of dihedral angles is controlled by the balancing of the two interfacial energies involved: the grain boundary energy between the two grains of the same phase, γ_b, and the energy of the interface between the two different phases, γ_i. For isotropic materials the angle is given by

$$\gamma_b = 2\gamma_i \cos(\Theta/2)$$

(Smith, 1948), but because most materials of interest to geologists have significant anisotropy of interfacial energy (e.g. Kretz, 1966; Vernon, 1968; Laporte *et al.*, 1997), the equation above is modified to incorporate torque forces that act to rotate interfaces to lower energy orientations (Herring, 1951*b*; Hoffman & Cahn, 1972; Cahn & Hoffman, 1974). This results in stabilization of planar interfaces at pore corners (e.g. Kretz, 1966; Vernon, 1968; Laporte & Watson, 1995; Cmíral *et al.*, 1998; Lupulescu & Watson, 1999; Laporte & Provost, 2000), and a range of possible equilibrium angles, depending on the relative orientation of the solid grains (Herring, 1951*b*; Laporte & Provost, 2000).

The low energy of solid–melt interfaces compared with typical grain boundary energies results in low dihedral angles with median values <60° (e.g. Waff & Bulau, 1979; Bulau, 1982; Toramaru & Fujii, 1986; von Bargen & Waff, 1988; Laporte, 1994; Faul, 1997; Wark *et al.*, 2003; Maumus *et al.*, 2004). The presence of curved interfaces, even in relatively anisotropic minerals such as amphibole (Vernon, 1968; Laporte & Watson, 1995; Lupulescu & Watson, 1999), shows that the anisotropy of geological materials may not be sufficient to stabilize completely faceted grains, and so the standard deviation from the mean dihedral angle is likely to be low. For example, the anisotropy of the anorthite–silicate melt system results in a standard deviation of ∼12° (Laporte & Provost, 2000). For completely solid aggregates, similarities in both the structure and composition of adjacent silicate phases lead to similar interfacial energies, and hence dihedral angles of ∼120°. Typical values fall in the range 100–140° (e.g. Kretz, 1966; Vernon, 1968, 1970; Fig. 2a). Standard deviations are generally in the range 10–20° (Vernon, 1968, 1970; Fig. 1).

As growth-controlled crystal forms and pore structures will tend to dominate during the early stages of solidification, when growth rates may be high, populations of dihedral angles in the early history of a mush are likely to be controlled by impingement. Subsequent modification of grain shape and pore structure driven by internal energy minimization will drive the population towards one of lower angle and lower standard deviation (Fig. 1). If the mush solidifies, with pseudomorphing of the porosity by a late-crystallizing phase (e.g. Platten, 1981; Harte *et al.*, 1991; Pattison & Harte, 1991; Holness & Clemens, 1999; Sawyer, 1999, 2001; Rosenberg & Riller, 2000; Holness & Watt, 2001), subsequent textural modification must drive the population of dihedral angles at the corners of the pseudomorphed pores away from the inherited distribution towards one of solid-state textural

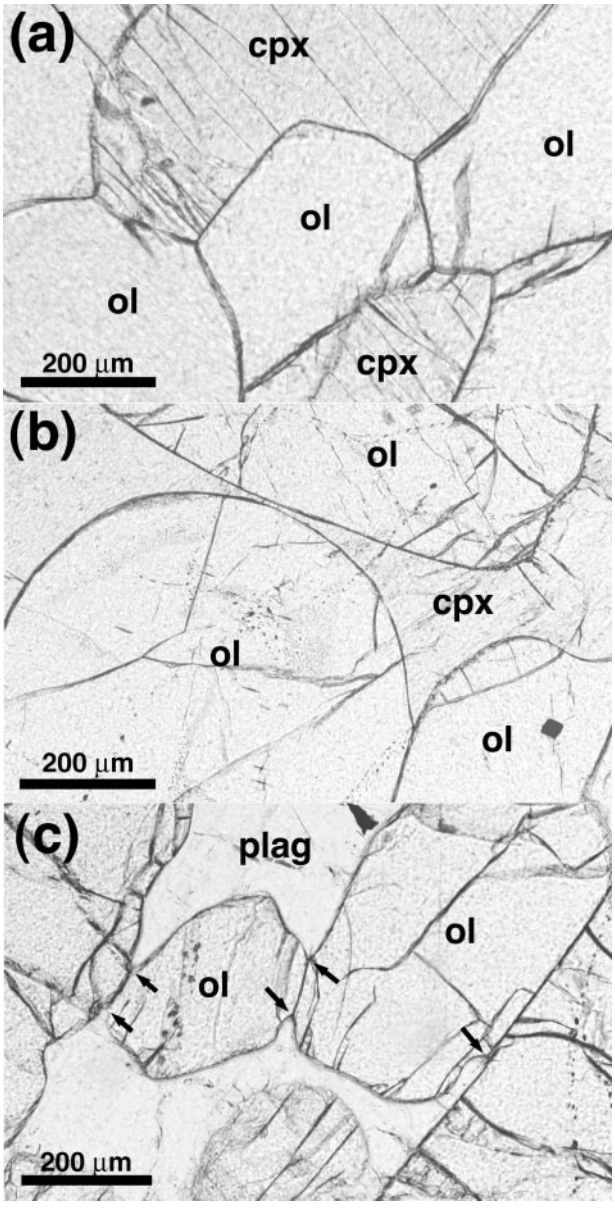

Fig. 2. (a) Mantle nodule entrained in alkali basalt. Eifel, Germany. The large grain size, smooth grain boundaries and the large dihedral angle subtended at the olivine–olivine–clinopyroxene junctions should be noted. Several of the grain boundaries have opened during eruption of the nodule. (b) Olivine cumulate from Rum with isolated, rounded olivine grains enclosed by poikilitic clinopyroxene. The low olivine–olivine–clinopyroxene dihedral angle should be noted. (c) Olivine cumulate from Rum, with isolated rounded olivine grains surrounded by plagioclase. The original low olivine–olivine–plagioclase dihedral angles have changed to higher angles (arrowed, although still not the equilibrium solid-state value). This figure can be viewed in colour on *Journal of Petrology* online.

equilibrium. For a pseudomorphed impingement texture this involves an increase of median angle and a decrease of the standard deviation (Fig. 1). For a pseudomorphed equilibrium texture, solid-state equilibration involves an increase in median, together with an initial increase in the standard deviation as different parts of the rock equilibrate at different rates (Fig. 1).

These changes in dihedral angle, either during melt-present textural equilibration of an original impingement texture, or during solid-state modification of an inherited angle population, represent a problem of great importance to metallurgy and there is a significant literature on the subject, most concerning the specific example of grain boundary grooving. Grain boundary grooving occurs when a grain boundary intersects the planar surface of an experimentally prepared sample at a high angle. At the surface of the sample, the initial solid–solid–vapour dihedral angle is 180°, higher than the equilibrium angle, which, for metals, is ~140–160° (e.g. Mullins, 1994). Textural equilibration proceeds by the formation of a groove along the exposed grain boundary by a combination of surface, grain boundary and volume diffusion, to establish the lower, equilibrium dihedral angle.

The theory underpinning the literature is based on the boundary condition of a fixed dihedral angle at the base of the evolving groove; that is, the instantaneous establishment of the equilibrium dihedral angle in the immediate vicinity of the pore corner (Mullins, 1957). According to the accepted theoretical framework, equilibration then involves the propagation of the new surface curvature outwards, together with a deepening of the groove. The shape of the groove remains constant as it grows. In theory, therefore, it should always be possible to observe the solid-state equilibrium angle in fully solidified cumulates, provided the observations are made at sufficiently high magnification. However, in solid cumulates displaying clear evidence of sub-solidus textural change, there is no evidence for the ubiquitous establishment of the solid-state equilibrium angle (Fig. 2). Instead, the angle is generally intermediate between that of the inherited solid–solid–liquid angle and the equilibrium solid-state angle. Preliminary examination of such junctions with the scanning electron microscope shows that this intermediate angle, which is established at the break in slope clearly visible with an optical microscope, extends to within 0·1 μm of the junction itself. We do not believe it is plausible that there is another change in slope in the immediate vicinity of the pore corner, establishing the equilibrium angle on scales smaller than 0·1 μm. Support for the idea that angles change via a continuous series of intermediate steps, rather than by the instantaneous establishment of the higher angle coupled with outwards propagation of the new surface curvature, is provided by high-magnification observations of tungsten surfaces (Zhang *et al.*, 2002). In this study we argue that change in dihedral angle occurs by a gradual process over a large (~10 μm) distance from the grain junction, without instantaneous establishment of the equilibrium angle, akin to the opening or closing of a book.

The importance of understanding the process of textural equilibration, quite apart from the physical fundamentals of the process, is the possibility of using partially equilibrated textures to calibrate the rates of geological processes. Because the extent to which the dihedral angle changes is a function of thermal history, if we understand the process we can obtain rate laws that will provide a temporal framework for textural evolution. Holness (2005) has shown that observed dihedral angles in cumulates from a single intrusion vary significantly. She suggested that these variations provide information about the rate of upwards movement of the solidification front and the influence of later influxes of hot replenishing magma into the chamber. A sound qualitative and quantitative understanding of the change in dihedral angle could thus be a powerful tool in understanding magma chamber evolution.

One of the aims of this study is to show that it is possible to determine, from dihedral angle populations and considerations of crystal shape, which end-member pore structure dominated the melt topology immediately prior either to complete solidification (for solidified cumulates that have not experienced later deformation or metamorphism), or to entrainment and eruption (for incompletely solidified igneous enclaves). We show that suites of related rocks lie on well-defined continua between an unequilibrated, growth-controlled, starting point and full textural equilibrium (at least in the immediate vicinity of pore corners and three-grain junctions). We also show that dihedral angle populations record information about late-stage crystal growth in open-system magma chambers and the sub-solidus cooling histories of cumulates. To achieve this we demonstrate that the currently accepted model for dihedral angle change is incorrect.

ANALYTICAL METHODS

Following the metallurgists, who pioneered work in this field using opaque materials, geologists have generally measured dihedral angles using a conventional, flat-stage, microscope or by analysis of images generated by scanning electron microscopy. This method relies on measuring a population of angles on a randomly oriented two-dimensional section through the material. For samples containing a single true value of the dihedral angle it can be shown that the median of a population of these angles is within 1° of the true three-dimensional (3-D) angle (Harker & Parker, 1945; Riegger & Van Vlack, 1960). For other samples, including those of geological interest, sophisticated statistical techniques are required to constrain the range of true equilibrium angles (e.g. Jurewicz & Jurewicz, 1986). Despite the fact that the problem can be neatly circumvented by the use of the Universal Stage on an optical microscope (Vernon, 1997), there have been very few published attempts to use this technique (e.g. Kretz, 1966; Vernon, 1968, 1970; Holness, 2005).

Given the effect of surface energy anisotropy, and the significance of the information contained within the actual population of true 3-D dihedral angles, we have concentrated exclusively on measurements obtained with a Universal Stage. We used a four-axis Leitz Universal Stage, mounted on a James Swift microscope. This combination permits up to 40° rotation of the thin-section from the horizontal, and allows accurate measurement of about half of the dihedral angles present in the sample, with an error on each measurement of a few degrees. We consider that this method can be used to obtain a representative population of angles in samples without a preferred crystal orientation. We measured between 30 and 110 angles in each sample, with a magnification of ×300.

The dihedral angles we have measured are those of either glass or the last-formed crystalline phase, in contact with a variety of solid phases (plagioclase, amphibole and clinopyroxene). The last-formed crystalline phase is generally clearly distinguishable as interstitial, and forms either small wedges of material between the earlier formed grains or large poikilocrysts. For comparison we have also measured dihedral angles in rocks that are probably at, or close to, textural equilibrium.

CHOICE OF SAMPLES

In an exactly analogous manner to metamorphic petrography, which is at least in part dependent on the observation of incomplete reactions, the decoding of textural evolution is reliant on the study of rock suites that have not attained textural equilibrium. For cumulate rocks, such suites are to be found in small magma chambers [e.g. the conduit-dominated fractionation in the Kula Volcanic Province, Western Turkey (Holness & Bunbury, in preparation)], or in larger magma chambers that are either subject to frequent disturbance by replenishment and eruption events (e.g. the 5 km diameter active open-system chamber underneath the Kameni Islands, Santorini, and the 8 km diameter open-system chamber of the Rum Igneous Complex), or in which cool, late-stage melts circulated (Skaergaard intrusion, Greenland).

Most of the samples studied form part of a continuing project on cumulate textural evolution (e.g. Holness, 2005) and come from the Isle of Rum, Scotland. The bulk of the 8 km diameter current exposure of this Palaeocene igneous centre comprises a series of well-defined layers of alternating peridotite (strictly these olivine cumulates are feldspathic peridotites) and feldspar-rich rocks [for a detailed description the reader is referred to Emeleus (1997)]. The latter comprise troctolites and gabbros, and are collectively known by the local name of allivalite. The sequence of crystallization in the Layered Suite of the Rum magma chamber was olivine (and

spinel) → olivine + plagioclase → olivine + plagioclase + clinopyroxene → minor hydrous phases (such as brown mica and amphibole). For this study we concentrate on samples from the eastern part of the Layered Suite.

Further samples are from the Quaternary Kula Volcanic Province in western Turkey. This continental rift terrane contains approximately 80 monogenetic volcanic cones (Richardson-Bunbury, 1996). The volcanism consists of small, alkaline, hydrous magma batches (each with a volume of $\sim 0{\cdot}01\,km^3$) generated by extension, with a plumbing system that generally solidifies completely between eruptions. However, a small subset of the cones contains abundant enclaves derived from the crystal mush developed on the margins of the plumbing system during fractionation of earlier erupted lavas (Holness & Bunbury, in preparation). The enclave population is dominated by almost monomineralic, glass-bearing, amphibole cumulates, some of which contain variable amounts of clinopyroxene and apatite.

Samples also include a group of glass-bearing andesitic enclaves from the Kameni Islands, Santorini. The Santorini volcano lies above a subduction zone, and the post-caldera lavas forming the Kameni islands are derived from a cool, long-lived, shallow magma chamber that has produced essentially identical dacitic lavas for the last 2000 years. The enclaves are thought to be derived from layers of aphyric replenishing magma intruded at the base of the active chamber (Martin *et al.*, 2003). Crystallization in the replenishing layer, driven by thermal equilibration with the resident dacite, resulted in a density inversion that precipitated convective overturn and eruption, with entrainment of incompletely crystallized andesitic enclaves (Martin *et al.*, 2003).

Samples of glass-bearing, crystal-rich, enclaves were collected from the basaltic Borgahraun flow from the Theistareykir segment of the Northern Volcanic Zone of Iceland. The host magma is Mg-rich ($\sim 12{\cdot}5$ wt % MgO), and K-poor, and was generated by large-fraction mantle melting on the ridge axis. It fractionated at depths of 20–30 km in the mantle before eruption, with a crystallization order olivine → olivine + clinopyroxene → olivine + clinopyroxene + plagioclase. The crystal-rich enclaves are small (<1 cm diameter) and include gabbros, wehrlites and troctolites [for details see Maclennan *et al.* (2003)].

The enclave suites were augmented by two Tertiary lavas from the Isle of Mull, Scotland. These felsic lavas (one a pitchstone, the other an innimorite) contain clots of plagioclase phenocrysts with fine-grained interstitial material. The matrix of neither rock is glassy, but is sufficiently fine-grained for the plagioclase grain boundaries to be clearly defined. A similar sample is from a picritic dyke from the Isle of Rum, collected by J. McClurg (McClurg, 1982) and generally known as M9 (e.g. Upton *et al.* 2002), which contains abundant clots of olivine set in a fine-grained matrix.

The final set of samples is a diverse group of coarse-grained material with the typical characteristics of textural equilibrium. It includes granulites, mantle nodules and cumulates from large mafic intrusions. This set of samples was used to determine the values of sub-solidus dihedral angles.

TEXTURAL OBSERVATIONS: GLASS-BEARING ROCKS

Kula

A set of enclaves was chosen containing abundant fresh glass and unaltered crystals. The amount of glass is variable, and heterogeneously distributed at the scale of a thin-section. Pockets rich in glass are adjacent to virtually glass-free regions. The crystalline phases are amphibole, clinopyroxene and apatite. The amphibole is a brown, pleochroic, compositionally zoned, kaersutite, commonly equant with well-formed crystal faces. The clinopyroxene is a titanium-rich diopside, forming equant, compositionally zoned grains. In some samples the amphibole grains display no change in surface curvature at two-grain junctions (Fig. 3a), suggestive of a dominance of growth kinetics in controlling the pore shape. However, in a few samples the amphibole forms clusters of rounded grains set in interstitial glass (Fig. 3b), with grain shapes more reminiscent of an approach to the equilibrium form [such as that developed by the smaller grains in the experiments of Lupulescu & Watson (1999)]. In these samples, the surfaces at many pore corners are curved.

Two sets of dihedral angle measurements were made: amphibole–amphibole–glass, and clinopyroxene–clinopyroxene–glass. It was possible to measure both in only four of the 11 enclaves examined. The amphibole–amphibole–glass dihedral angles show great variability between enclaves. Those with little sign of surface curvature at two-grain junctions provide a population with a median of $\sim 60°$ and a standard deviation of $\sim 25°$, whereas those with rounded grains and some surface curvature at pore corners have a much lower median dihedral angle of $\sim 30°$ and a correspondingly low standard deviation of $\sim 16°$. Most of the samples fall between these two endpoints.

The clinopyroxene–clinopyroxene–glass dihedral angles also show variability between enclaves, with the range of median values from 39° to 65°. The standard deviation is in the range 18–22°, with no correlation with the median. Clinopyroxene generally has a higher median value of dihedral angle than the coexisting amphibole.

Santorini

The andesitic enclaves from the dacite lava flows forming the Kameni Islands contain up to 50 vol. % glass, with a

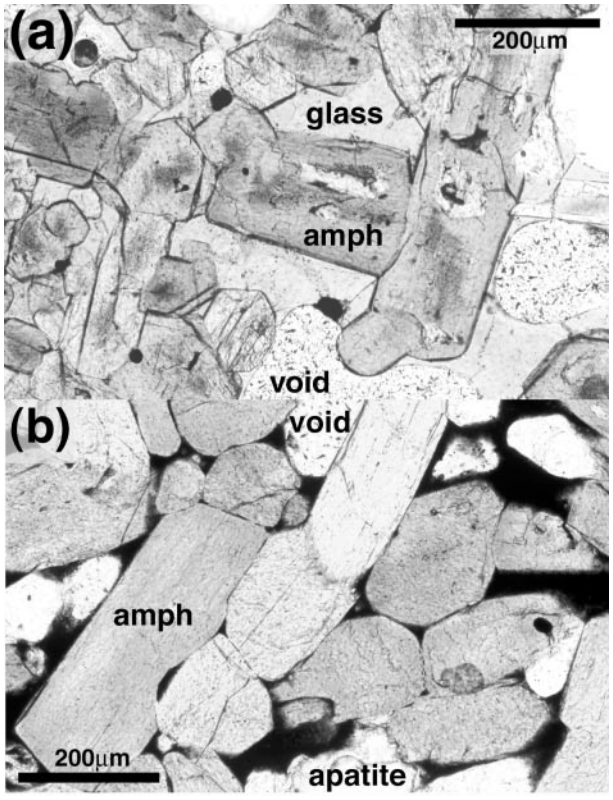

Fig. 3. Glass-bearing amphibole cumulates found as enclaves in alkali basalts from the Kula Volcanic Province, Western Turkey. (a) In several enclaves, the junctions between amphibole grains show no signs of development of curvature. This enclave contains abundant pale brown glass, with euhedral, compositionally zoned, amphibole grains with flat faces and impingement textures. (b) This enclave contains opaque glass, with rounded grains of amphibole. The amphibole–amphibole–glass dihedral angle is low. The presence of curved interfaces at two-grain junctions should be noted. This figure can be viewed in colour on *Journal of Petrology* online.

crystalline fraction dominated by a coarse framework of elongate, tabular plagioclase crystals (Fig. 4a), and subsidiary clinopyroxene and titanomagnetite. Adjacent plagioclase crystals in the framework have well-defined grain boundaries, with grain clusters suggestive of a certain degree of heterogeneous nucleation. The edges of the plagioclase grains are marked by a well-defined outer zone of slightly more albitic material ($An_{20–60}$ compared with the core composition of $An_{50–71}$), which is clearly visible optically (Fig. 4c and d). The ends of most of the plagioclase grains have hopper-like extensions, which appear as elongate extensions in thin-section (Fig. 4b), and occur entirely within the marginal zone. Close inspection of the contacts between any two plagioclase grains reveals the development of surface curvature on the otherwise planar crystal faces (Fig. 4c): some junctions have deep incisions along the grain boundary. These incisions are deepest where the junction between the two grains is at a low angle, and always occur entirely within the marginal zone (Fig. 4c and d). They are identical in form to features developed in biotite–silicate melt aggregates during quenching of experimental run products (Laporte & Watson, 1995). Following Laporte & Watson (1995), we interpret the incisions as a result of diffusion-limited growth during a period of rapid crystallization, linked most plausibly to the quenching involved in convective overturn of the andesitic layer. Measurement of the angle developed within the incisions at junctions between two plagioclase grains results in a wide range of populations with medians of 32–51°, with corresponding standard deviations of 13–28°.

Because the quench growth is clearly visible optically, the Kameni enclaves also provide an opportunity to determine what the angles were before the rapid growth event. Measurement of the angle subtended between adjacent plagioclase grains far from their mutual junction results in a population with a median angle of ~60°, and a standard deviation of 25–30°.

TEXTURAL OBSERVATIONS: CRYSTAL CLOTS IN LAVAS

Iceland

The small enclaves and crystal clots show great variation of both modal composition and texture (Maclennan *et al.*, 2003). Some are fully crystalline, whereas others contain glass. In the troctolitic and gabbroic clots, olivine forms rounded to sub-rounded grains, commonly showing undulose extinction indicative of deformation, in a matrix of tabular plagioclase. The plagioclase has neither quench growth nor development of surface curvature. Clinopyroxene is commonly interstitial, and in some samples incompletely fills the otherwise glass-bearing porosity.

Dunitic crystal clots, composed entirely of olivine, tend to show signs of textural equilibration such as rounding of grains and smooth, curved, surfaces near pore corners (Fig. 5a). In these enclaves, the olivine–olivine–glass dihedral angles form a population with a median of 27° and a standard deviation of 13°.

Rum

The picritic dyke, M9, contains abundant olivine phenocrysts and glomerocrysts. Although many of the olivine grains have prominent crystal faces, they also have curved regions, indicative of an approach to the equilibrium form (Fig. 5b). In particular, many of the grain junctions show surface curvature.

The groundmass of M9 is commonly assumed to be a possible parental magma for the Layered Suite on Rum (e.g. McClurg, 1982; Upton *et al.*, 2002). As such, the olivine–olivine–groundmass dihedral angle population is a plausible contender for the olivine–olivine–melt angle

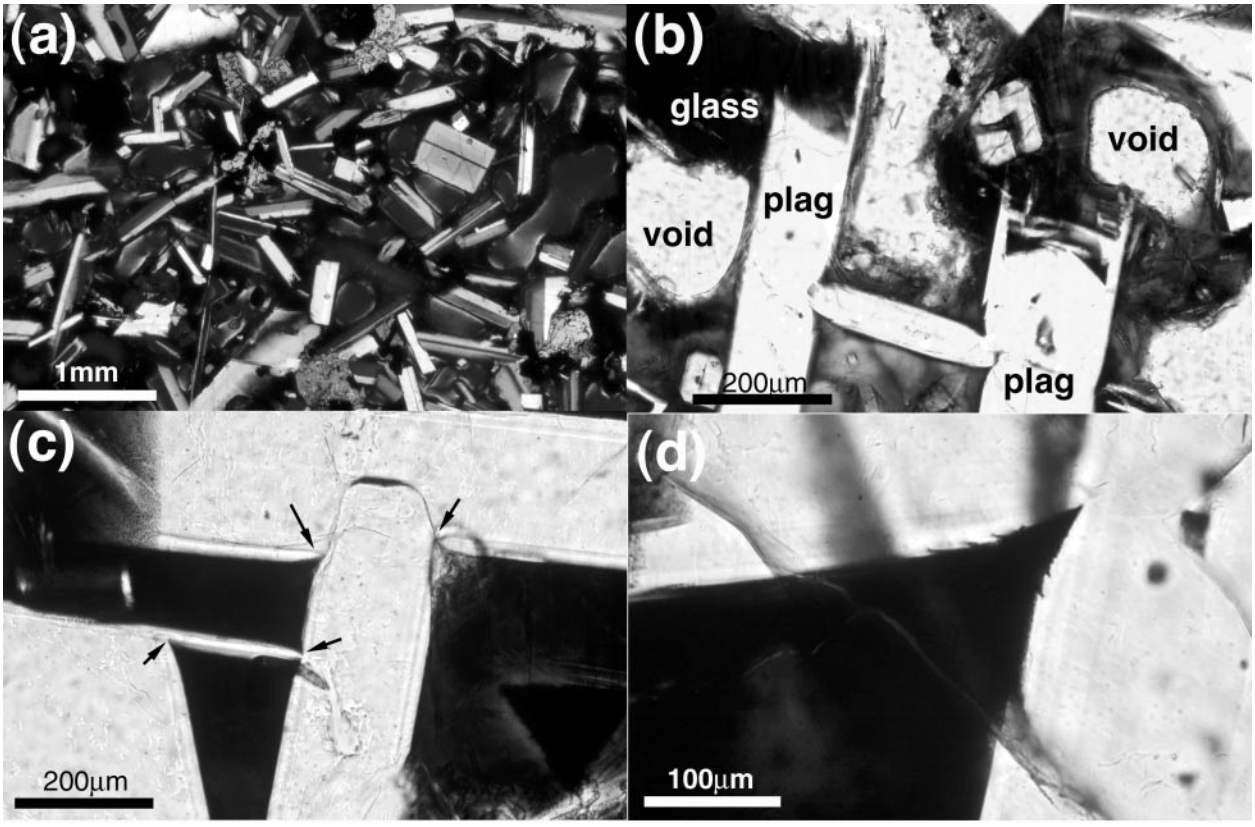

Fig. 4. (a) Andesitic enclave from the Kameni Islands, Santorini. Crossed polars. The isotropic (black) matrix is dominated by fresh glass but contains abundant vesicles. The solid phases are euhedral, twinned plagioclase, irregular grains of clinopyroxene and opaque titanomagnetite (not visible). (b) Three plagioclase grains, with the larger two (oriented north–south) showing evidence of hopper-like extensions as a result of rapid growth during a quench phase. (c) Close-up of the junction between several plagioclase grains. The arrows show where the junctions have been modified by changes in surface curvature caused by diffusion-limited crystal growth. The junction at the top right is obscured by a small clinopyroxene grain. The distribution of apparent angles in the initial impingement texture was obtained by measuring the angles between the planar, non-curved parts of the grains. The pale grey lines that mark the boundary between the original crystals and the quench-related growth should be noted. (d) Close-up of a two-grain junction showing the irregularities of the curved surface. These are small versions of the hopper-like extensions shown in (b). This figure can be viewed in colour on *Journal of Petrology* online.

in this magma type. It forms a population with a median of 29° and a standard deviation of 14°.

Mull

Clots of plagioclase crystals in the two Mull lavas (Fig. 5c) include crystals with variable shapes, although all show some areas of curvature. In particular, the corners of the generally tabular grains are curved, in contrast to the complete lack of curvature on the pre-quench shape of the Kameni plagioclase. We consider that this difference in shape reflects a difference in the extent of equilibration between the two sets of samples, with the Kameni crystal shape dominated by growth, and the Mull crystal shape indicating progress towards equilibrium. Curved two-grain junctions are common. Both samples yield indistinguishable populations of plagioclase–plagioclase–groundmass dihedral angles with a median of 27–28° and standard deviation of 15°.

TEXTURAL OBSERVATIONS: GLASS-FREE CUMULATES

The samples in this category are all from the Rum Layered Suite. We confined observations to two pairs of minerals: olivine–clinopyroxene, and plagioclase–clinopyroxene. The olivine–clinopyroxene observations were made exclusively on the peridotite members of the Layered Suite. In these rocks the olivine forms cumulus grains, which range from high aspect-ratio plates to more equant forms, commonly aligned to form a pronounced igneous layering with evidence of intracrystalline deformation linked to compaction (e.g. Hunter, 1996; Barnes & Maier, 2002). The intercumulus phase is either plagioclase or clinopyroxene. The clinopyroxene commonly forms large poikilocrysts enclosing several hundred olivine grains. Some of these enclosed grains are smaller and spaced further apart than olivine grains outside the poikilocryst. Pockets of primary magmatic hydrous

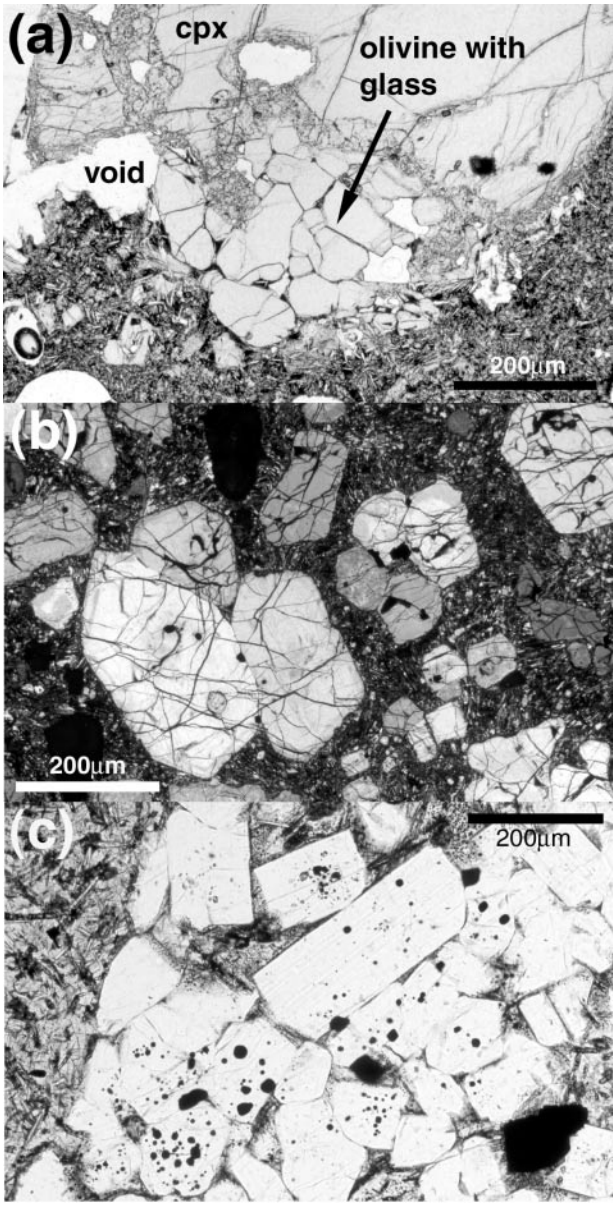

Fig. 5. Photomicrographs of crystal aggregates in lavas. (a) Wehrlitic fragment in a lava flow from Theistareykir, Iceland. The olivine aggregate contains glass-filled pores. (b) Olivine-phyric picritic dyke from Rum, collected by J. McClurg and known as M9 (McClurg, 1982). (c) Clot of plagioclase grains (with some inclusions of opaque oxide grains) in a pitchstone from Mull. The melt in the pores of the plagioclase aggregate has crystallized to a fine-grained matrix. The more rounded shape of the grains compared with the plagioclase grains illustrated in Fig. 4 should be noted. This figure can be viewed in colour on *Journal of Petrology* online.

minerals are generally found on the margins of the poikilocrysts, suggesting that progressive growth of the intercumulus clinopyroxene and plagioclase concentrated the last, H_2O-enriched melt at the poikilocryst margins.

The medians of populations of olivine–olivine–clinopyroxene dihedral angles in the peridotites are generally low, ranging from 40 to 100°, with standard deviations between 20° and 30°. The junctions with low observed angles have smoothly curved olivine–clinopyroxene grain boundaries (Fig. 2b) whereas those with higher observed angles have a change in curvature as the junction is approached (e.g. Fig. 2c).

Spatial information on the variation of olivine–olivine–clinopyroxene dihedral angles is provided by detailed analysis of single, large poikilocrysts. Figure 6 shows a drawing of a region of peridotite in which the interstitial material is formed of three contiguous clinopyroxene poikilocrysts. All possible dihedral angles were measured (allowing for the common presence of thin films of clinopyroxene separating olivine grains, minor alteration and the maximum rotation capacity of the Universal Stage mounted on the James Swift microscope). Those from the very edges of the poikilocryst form a population with a median of 38° and a standard deviation of 23°, those from the outermost zone (arbitrarily chosen, and shown in Fig. 6) have a median of 67° and a standard deviation of 24°, and those from the central part have a median of 75° and a standard deviation of 23°. Although we cannot be sure of the 3-D shape of the poikilocrysts, the observed increase in median angle from the edges to the central (at least in the plane of the thin-section) region is significant (according to the Mann–Whitney *U* test).

The range of olivine–olivine–clinopyroxene dihedral angles in a texturally equilibrated rock was determined from a coarse-grained, non-deformed mantle nodule from the Eifel in Germany. This gave a median value of 115° with a standard deviation of 16°.

The gabbroic allivalites are dominated by cumulus clinopyroxene with laths of plagioclase. A pronounced igneous foliation is defined by the alignment of plagioclase. The cumulus clinopyroxene grains commonly have elongate extensions along plagioclase–plagioclase grain boundaries (Fig. 7a). In the troctolitic members of the allivalite horizons, the cumulus phases are olivine and plagioclase. Clinopyroxene forms interstitial wedges between plagioclase laths, or continuous rinds around cumulus olivine grains (Fig. 7b). Clinopyroxene may also form large (up to 1 cm diameter) poikilocrysts enclosing randomly oriented plagioclase grains. The igneous foliation wraps around these poikilocrysts.

The plagioclase–plagioclase–clinopyroxene angle in the allivalites, both gabbroic and troctolitic, has been studied in detail by Holness (2005). The median value ranges from about 60° (SD ~25°) to 110° (SD ~20°), with variations in dihedral angle from the base to the top of individual allivalite units. Most of each allivalite unit has a relatively constant population of dihedral angles (with medians in the range 80–90°) with the topmost few decimetres showing an increase in angle ascribed to the thermal effects of the overlying peridotite (Holness, 2005). The base of some allivalite horizons has much

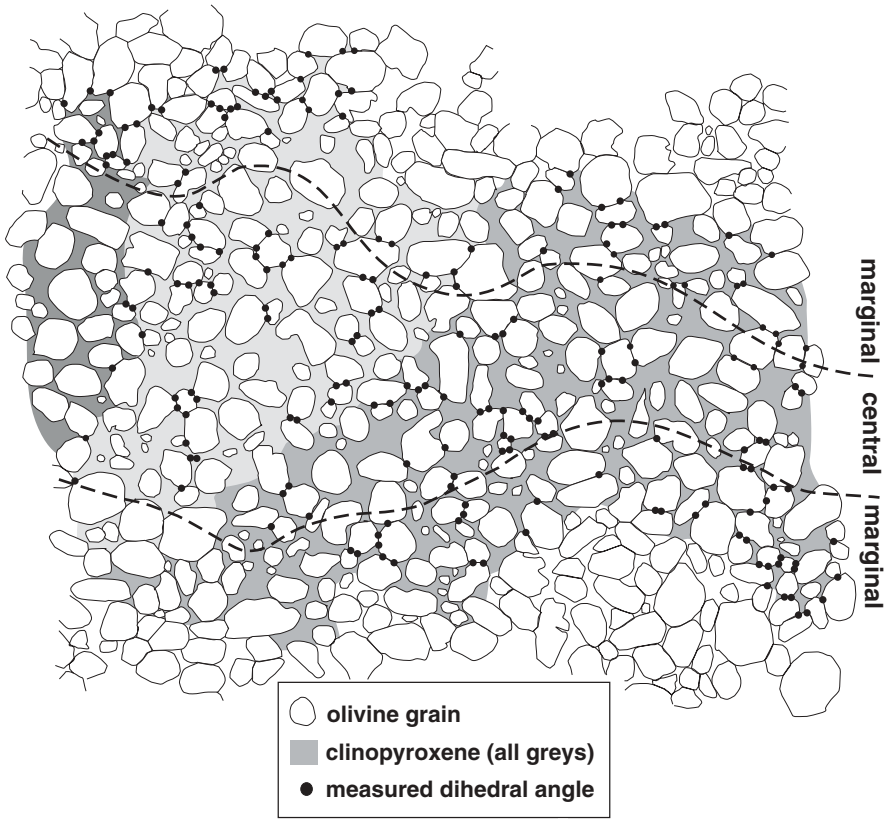

Fig. 6. Line drawing of an olivine cumulate with the cumulus grains enclosed by either large clinopyroxene oikocrysts (shown as various shades of grey) or fine-grained plagioclase (shown at the margins of the figure as a white background to the outlined olivine grains). The dots show the position of measured olivine–olivine–clinopyroxene dihedral angles. The division of the poikilitic grains into marginal and central regions is arbitrary.

lower angles, down to median values of 65–70°, thought to be due to late-stage infiltration of melt from underlying horizons (M. B. Holness, unpublished data, 2004). In the vicinity of a large, late-stage, peridotite intrusion, dihedral angles depart significantly from this pattern, with large variations in the median values from the expected constant range of 80–90° (Holness, 2005).

There is no correlation between bulk composition (in particular, the modal amount of clinopyroxene) and dihedral angle. There is no correlation between dihedral angle and whether the clinopyroxene is interstitial or cumulus. In common with the poikilocrysts in the peridotites, the central regions of clinopyroxene poikilocrysts in the allivalites have significantly higher plagioclase–plagioclase–clinopyroxene dihedral angles (with medians >100°) than the interstitial material outside the poikilocrysts (medians ~90°). The higher angles are associated with rounding of the corners of the plagioclase grains. This points to a greater extent of textural equilibrium in the centres of the poikilocrysts compared with outside (e.g. Kretz, 1966; Vernon, 1968).

The equilibrium population of plagioclase–plagioclase–clinopyroxene dihedral angles was determined from a texturally equilibrated granulite (sample 11787, Harker Collection, Cambridge University, collected from Perugar, Madura district, south India). A population of 100 true 3-D angles ranged from 68° to 150°, demonstrating a significant crystallographic control (i.e. interfacial energy anisotropy) on the position of the grain boundaries in clinopyroxene–plagioclase aggregates. The population is unimodal, with a median of 114°, a mode of 116°, and a standard deviation of 17°. These results are consistent with those of Vernon (1968, 1970; Fig. 7).

INTERPRETATION OF TEXTURAL OBSERVATIONS

Crystal clots in lavas

The measurements of solid–solid–melt dihedral angles determined from the crystal clots in lavas are indistinguishable, with medians of 27–28° and standard deviations of 13–15°, despite the range of crystalline solids (olivine and plagioclase) and magma composition (basic and silicic). Although the dataset is small, this represents a

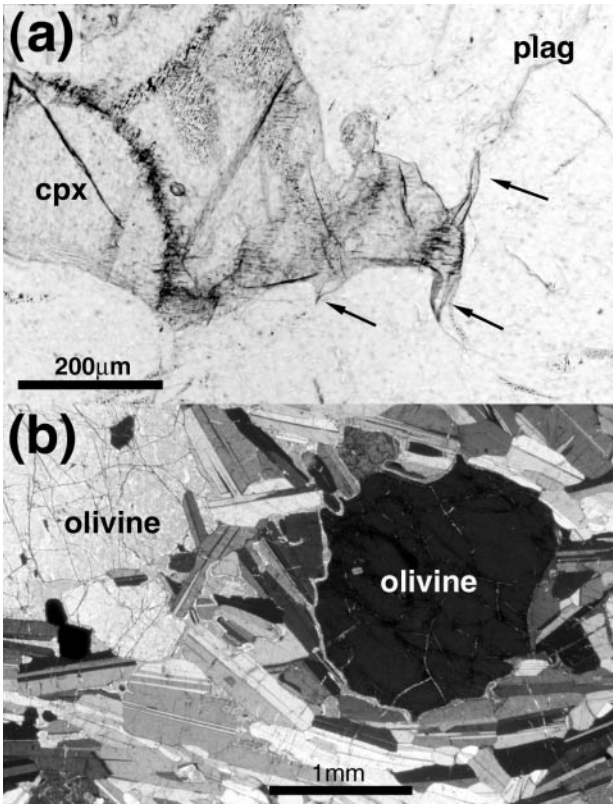

Fig. 7. Photomicrographs of Rum allivalites. (a) Cumulus clinopyroxene grains in the gabbros have elongate extensions along plagioclase–plagioclase grain boundaries (arrowed), which have low plagioclase–plagioclase–clinopyroxene dihedral angles. (b) Typical view of a Rum allivalite, with large cumulus olivine grains, aligned cumulus plagioclase grains, and interstitial clinopyroxene. It should be noted that the clinopyroxene is optically continuous over large areas and that it forms a rind separating olivine from plagioclase. This figure can be viewed in colour on *Journal of Petrology* online.

departure from previously reported results from experimental determinations of dihedral angle, which vary widely, even for the same solid–melt combination. For example, for anorthite–silicic melt, Longhi & Jurewicz (1995) reported a mean angle of 45°, whereas Laporte *et al.* (1997) reported a mean of 28°, with a standard deviation from the mean of 12° (Laporte & Provost, 2000). This last result is indistinguishable from our measurements of plagioclase–plagioclase–melt angles in natural samples. In contrast, our value for the median olivine–olivine–melt dihedral angle lies in the middle of the range of experimental median values, which range from 49° (Toramaru & Fujii, 1986) to 0–10° [Cmíral *et al.* (1998), although Laporte & Provost (2000) considered their reporting to be biased towards lower angles].

The reason for the wide range in published values is unlikely to reflect the effects of the small differences in melt composition between different studies. Laporte (1994) reported lower angles for wet melts compared with dry melts, and although this may account for the large difference between the result of Longhi & Jurewicz (1995) (45° for a dry melt) and Laporte *et al.* (1997) (28° for a wet melt), we consider it possible that high reported angles reflect a departure from textural equilibrium in the experimental charges, with some control of pore geometry by crystal growth. It is perhaps significant that the lowest angles for the olivine-basalt system [even accounting for the bias pointed out by Laporte & Provost (2000)] are derived from unusually long experimental durations (Cmíral *et al.*, 1998), and it is highly likely that the presence of H_2O in the melt will enhance diffusion and thus equilibration rates, resulting in lower angles for similar run durations for the anorthite–melt system. We consider it plausible that magmas erupted from large chambers, in which cooling rates were slow, are likely to contain crystal clots with pore geometries with a close approach to equilibrium.

In any case, the general similarity of our observations of solid–solid–melt dihedral angles to those obtained from experimental determinations of solid–solid–melt angles in silicate systems gives us confidence that we have a good constraint on the equilibrium position for melt-bearing silicate systems. Melt-bearing equilibrium results in a low median solid–solid–melt dihedral angle and a low standard deviation (Fig. 8). This contrasts with solid-state equilibrium, which results in a high median angle and low standard deviation, with a range of possible populations dependent on which crystalline phases are involved. The range of median and standard deviations in previously published studies (Vernon, 1968, 1970) is shown in Fig. 8, with our results for comparison.

Given this information we are now in a position to compare textural data from a range of environments to determine their degree of approach to textural equilibrium. We begin this process with the glass-bearing enclaves from Kula and Santorini. These provide us with the opportunity to constrain the actual melt topology in the last stages of solidification.

Glass-bearing enclaves: super-solidus textural evolution

The medians of the amphibole–amphibole–glass and clinopyroxene–clinopyroxene–glass dihedral angle populations from the Kula enclaves are plotted against standard deviation in Fig. 9. These form a linear trend between an end-member represented by those samples in which the grains show neither deflections at pore corners nor rounding, and one represented by the group of texturally equilibrated crystal clots in lavas. The results from the Kameni enclaves of Santorini are also plotted in Fig. 9. The populations from this enclave suite again form a trend, similar to that from Kula, with the samples at the lower end of the trend indistinguishable from those from Kula.

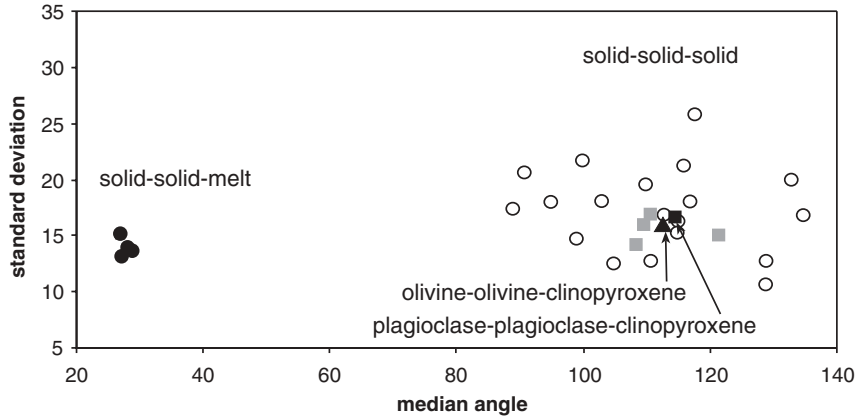

Fig. 8. Comparison of populations of true 3-D dihedral angles for equilibrated melt-bearing textures (•) and solid textures. The melt data were collected as part of this study. ○, solid data from Vernon (1968), measured in granulite-grade metamorphic rocks. Grey squares, solid data from plagioclase–plagioclase–clinopyroxene populations measured in granulites (Vernon, 1970). ■, the granulite plagioclase–plagioclase–clinopyroxene population measured as part of this study [indistinguishable from that of Vernon (1968)]. ▲, the olivine–olivine–clinopyroxene population measured as part of this study.

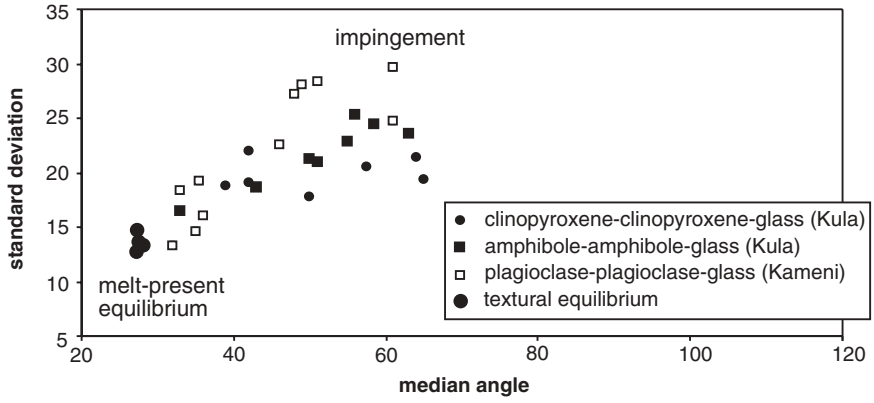

Fig. 9. Comparison of populations of true 3-D dihedral angles measured in glass-bearing enclaves from Kula and the Kameni Islands (Santorini). The enclave dihedral angle populations form a trend from high median and standard deviations towards the melt-bearing equilibrium.

Given the association of decreasing dihedral angle with grain rounding in the Kula enclaves, we suggest that the Kula enclave suite records a continuous progression of textural change from an initial impingement texture, controlled only by the kinetics of crystal growth, towards one controlled by textural equilibrium (Fig. 9). The initial angle distribution is very broad, with a high median value. Progress towards textural equilibrium involves a gradual and continual process resulting in the movement of the population towards lower angles. The amphibole–melt dihedral angle has been determined experimentally to have a median of 25°, although no 3-D statistics are available (Laporte & Watson, 1995). Our observations suggest that the textural evolution of the glass-bearing amphibole enclaves involves a decrease of dihedral angle towards a median of 27–28° with a standard deviation of ∼14°. Those enclaves entrained and erupted during crystal growth contain unmodified impingement textures, whereas those in which a period of textural equilibration occurred before entrainment record successively lower median values and standard deviations.

In contrast, the trend of decreasing dihedral angle in the Kameni enclaves cannot be attributable to a process of textural equilibration. This is because the decrease in plagioclase–plagioclase–melt dihedral angle is associated with an increasing importance of diffusion-limited growth during a period of rapid crystallization (quenching). The trend from the initial impingement texture reflects a variable effect of such quenching. That this process results in a very similar trend to progressive equilibration provides a salutary reminder that dihedral angles must be considered in conjunction with considerations of grain shape and interfacial curvature. The difference in the underlying cause of changes in dihedral angle is apparent from the crystal shape. Whereas in the Kula enclaves, reduced angles are associated with rounding,

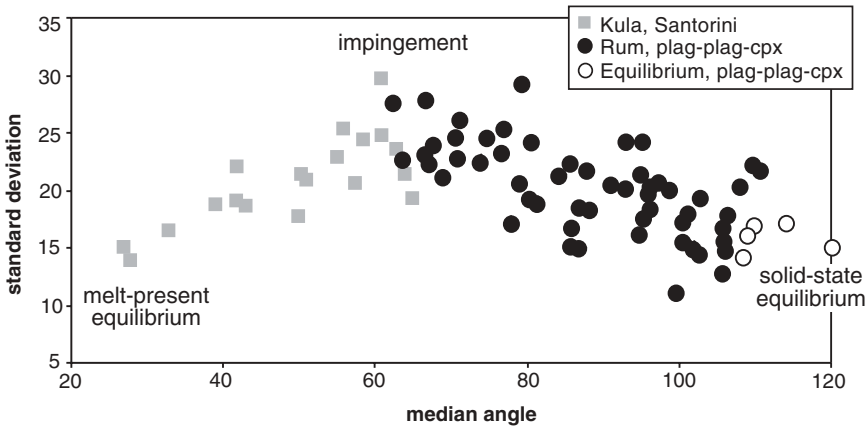

Fig. 10. Populations of true 3-D clinopyroxene–plagioclase–plagioclase dihedral angles from Rum allivalites (both troctolite and gabbro), compared with the amphibole and clinopyroxene data from the enclaves shown in more detail in Fig. 9. ○, the populations measured in granulites (Vernon, 1968, 1970; Holness, 2005).

the Kameni plagioclases always have quench-related, hopper-like, overgrowths, which are clearly growth-controlled and not part of the equilibrium form. That the two processes result in indistinguishable populations at low median angles simply reflects the fact that both trends must go through the origin.

It is also important to point out that although the establishment of low dihedral angles during textural equilibration is associated with a rounding of crystal shape and the establishment of minimum energy surfaces, changes in dihedral angle occur at a faster rate than changes in crystal shape (e.g. Laporte & Watson, 1995), especially for coarse-grained samples (e.g. Lulupsecu & Watson, 1999, fig. 4). We would not expect, therefore, an equilibrium dihedral angle always to be associated with the attainment of minimum energy surfaces throughout the aggregate, especially for the larger grains, but would expect to see at least some modification of grain shape and surface curvature.

What do these results imply for the evolution of cumulates? The textural observations from the glass-bearing enclaves demonstrate that it is possible to tell whether the pseudomorphing, interstitial phase in completely solidified cumulates inherited an impingement porosity or a more texturally equilibrated porosity (we consider it unlikely that the quench-modified porosities identified in the Kameni enclaves will be applicable to cumulates). We now discuss the dihedral angle populations in the Rum cumulates in the light of this.

Cumulates: sub-solidus textural equilibration

Figure 10 shows the median and standard deviation of the plagioclase–plagioclase–clinopyroxene angles in the Rum allivalites. These form a continuous elongate field linking the impingement end-member (defined by Kula amphibole and clinopyroxene and Kameni plagioclase) with the solid-state equilibrium position. Comparison of frequency plots for glass-bearing enclaves with those from the Rum allivalites demonstrates that the samples with the lowest median angles from Rum have dihedral angle populations that are indistinguishable from impingement textures. We infer that the starting texture for the clinopyroxene in the allivalites (i.e. the interstitial material in the troctolites, and the elongate apophyses emanating from the cumulus grains in the gabbros) was controlled entirely by the impingement of plagioclase.

This conclusion is reinforced by an examination of the gabbroic enclaves in the Icelandic lava. In these enclaves the plagioclase grains have well-developed crystal faces defining the shape of the interstitial clinopyroxene (Fig. 11a). There are also significant numbers of plagioclase crystal faces defining the shapes of interstitial clinopyroxene in the Rum allivalites (Fig. 11b), although the slower cooling of the latter has permitted significant sub-solidus textural modification. What is clearly discernible in the Icelandic enclaves has been modified almost to the point of being unrecognizable in the Rum allivalites. Figure 12 shows a selection of frequency plots for the population of Rum allivalites shown in Fig. 10. It is suggestive of a continuous process of angle change, with the initial broad spread of angles tightening and moving towards equilibrium. In this case, however, equilibrium involves an increase, rather than a decrease, in median angle.

The effect of compaction on the porosity of a melt-bearing crystal mush merits mention here. Critically, the Kameni enclaves show no signs of compaction—the plagioclase grains are randomly oriented. There is a similar lack of alignment of the plagioclase in the Icelandic enclaves. The similarity of the consequent impingement

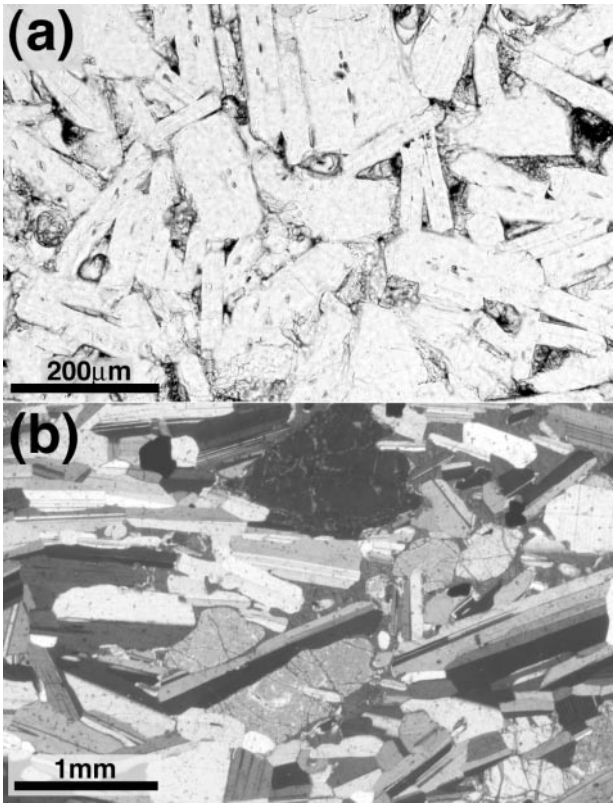

Fig. 11. (a) Photomicrograph under plane-polarized light of a gabbroic enclave from Iceland. Plagioclase grains with well-defined crystal faces form a framework with interstitial clinopyroxene. The low apparent plagioclase–plagioclase–clinopyroxene dihedral angles are a function of the angle of impingement of the plagioclase. (b) Typical troctolitic allivalite from Rum under crossed polars, with sub-rounded cumulus olivine grains and elongate cumulus plagioclase grains. The interstitial clinopyroxene has a shape controlled by the crystal faces of the adjacent plagioclase. This figure can be viewed in colour on *Journal of Petrology* online.

angle population of these uncompacted samples to the initial population of the Rum allivalites suggests that the Rum allivalites were not significantly compacted at the time of clinopyroxene nucleation. The common presence of a strong alignment of plagioclase in the Rum allivalites (e.g. Fig. 7b) suggests that (?shear-enhanced) compaction did indeed occur (e.g. Lo Ré *et al.*, 2003). However, clinopyroxene is commonly concentrated near cumulus olivine grains, where the plagioclase does not show a strong alignment. The strongest alignment of plagioclase is found in essentially clinopyroxene-free regions (Fig. 11b). We suggest that shear-enhanced compaction and alignment of plagioclase reduced the residual porosity everywhere except near olivine grains. The large olivine grains locally held open the plagioclase framework, preventing alignment of plagioclase and resulting in a heterogeneous distribution of melt, and hence clinopyroxene, with a non-compacted, random, initial impingement angle distribution.

The olivine–olivine–clinopyroxene angles from the Rum peridotites are shown in Fig. 13, annotated to show populations obtained from different regions of the poikilitic pyroxene grain depicted in Fig. 6. Although the olivine–olivine–clinopyroxene angles also show a range between low and high angles, the low angles are much lower than the plagioclase–plagioclase–clinopyroxene angles in the Rum allivalites. We suggest that these lowest angles are inherited from a texturally equilibrated melt-bearing precursor. Support for this comes from observations of individual grain junctions. Those with the lowest dihedral angle have smoothly curved olivine grains, consistent with the olivine grains being in equilibrium with the interstitial melt phase (Fig. 2b). At the time of crystallization of the clinopyroxene (and final solidification), the topology of the interstitial melt in the peridotites was thus fundamentally different from that immediately prior to complete solidification in the adjacent allivalites.

RATES AND MECHANISMS OF CHANGES IN DIHEDRAL ANGLE

We have shown that it is possible to differentiate between melt-bearing equilibrium and impingement textures using the population of true 3-D dihedral angles. We have also shown that suites of related rocks show a variety of dihedral angle populations intermediate between textural disequilibrium and equilibrium. This is contrary to the accepted theory of change in dihedral angle, which is based on the assumption of an instantaneous establishment of the equilibrium dihedral angle at the pore corner (Mullins, 1957). Evidence that dihedral angle change is effected by the movement of grain boundaries on a length-scale of $\sim$10 μm is provided in Fig. 2c. Here the olivine–plagioclase grain boundaries show marked changes of curvature some distance from the olivine–olivine–plagioclase boundary, with essentially planar interfaces at the junction. The angle between these, the observed dihedral angle, is greater than the olivine–olivine–melt angle, but less than the solid-state equilibrium angle. According to the theory developed for the establishment of grain boundary grooves (Mullins, 1957), this observed angle should actually be the solid-state angle.

We suggest that the underlying assumption of constant dihedral angle used by Mullins (1957) in constructing the theory of grain boundary grooving is incorrect. Instead, we suggest that the establishment of a new dihedral angle, either at the high-angle intersections of a grain boundary with an initially planar interface (i.e. grain boundary grooving), at the junction formed by impingement of growing crystals, or consequent to the replacement of melt by a solid, occurs by a gradual process involving the swinging round of relatively large areas of interface, in the manner of an opening or closing book.

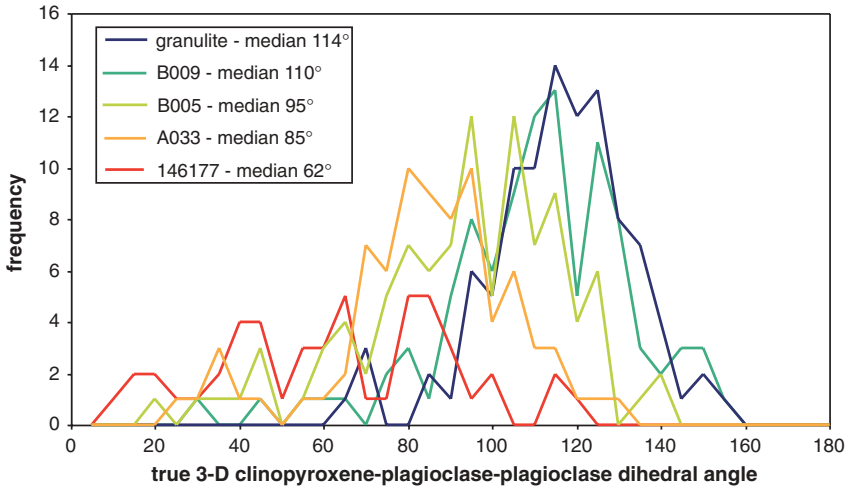

Fig. 12. Typical frequency plots for Rum allivalites, both gabbroic (B009) and troctolitic (A033, B005, 146177) compared with the solid-state equilibrium population observed in a granulite.

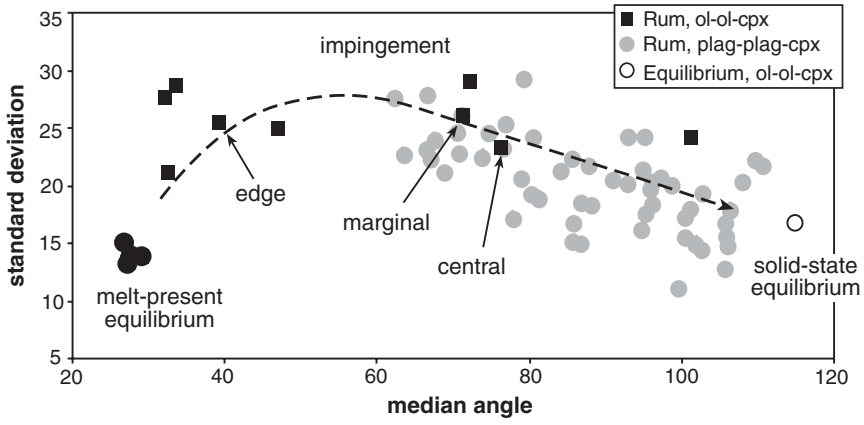

Fig. 13. Populations of true 3-D clinopyroxene–olivine–olivine dihedral angles in peridotitic cumulates of Rum compared with the equilibrium melt–olivine–olivine angles (•), the clinopyroxene–plagioclase–plagioclase angles from the Rum allivalites and the solid-state equilibrium clinopyroxene–olivine–olivine population measured as part of this study. The poikilitic clinopyroxene grain in Fig. 6 has distinct variations in populations for the different regions—the edgemost angles are generally lower than those in the rest of the grain. The dashed line shows a suggested trajectory for dihedral angle populations during the progression from an inherited pore structure towards solid-state equilibrium.

None of the work based on the Mullins model of grain boundary grooving (all of which is published in the metallurgical literature) has challenged the assumption of a constant dihedral angle. However, recent advances in surface imaging (such as atomic force microscopy) have provided the opportunity to measure the dihedral angle formed at the base of the grain boundary grooves, which are typically extremely small (a few microns wide and ~0·1 μm deep) in the metallurgical experiments. This new work, by Zhang *et al.* (2002) and Sachenko *et al.* (2004), shows that the dihedral angle does in fact decrease with groove evolution in tungsten, from the initial 180° to 150° by the end of the experiment, with a decreasing rate of angle change with time. However, the assumption of constant dihedral angle was not questioned in these studies. Instead they suggested that the surface energies are changing during the experiment as a result of changes in surface composition (Zhang *et al.*, 2002; Sachenko *et al.*, 2004). Evidence that the variety of angle populations observed in suites of related rocks are actually individual snapshots of a continuous process is provided by detailed observation of single poikilocrysts in the Rum peridotites.

The clinopyroxene poikilocrysts grew outwards from a central nucleus, with a concentration of the last-solidified melt identifiable by the concentrations of primary hydrous magmatic phases at the poikilocryst margins. This means that the central region of the poikilocryst is the oldest, with the margins having formed last. The olivine–olivine–clinopyroxene dihedral angle population in the central part of the poikilocryst is significantly closer to

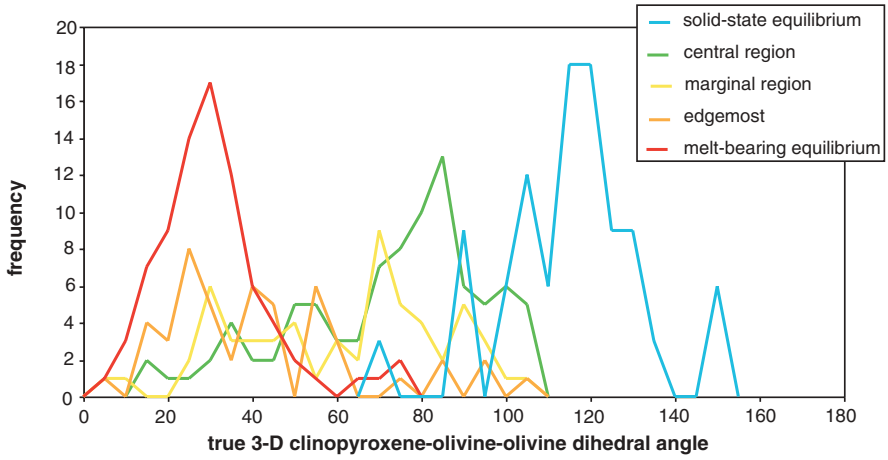

Fig. 14. Populations of true 3-D clinopyroxene–olivine–olivine dihedral angles in a single poikilitic clinopyroxene grain (shown in Fig. 6), compared with melt-bearing and solid-state equilibrium.

solid-state equilibrium than that of the margins, which is close to a plausible equilibrated olivine–olivine–melt starting position (Fig. 14). This is clear from the curvature of the olivine grain boundaries: at the margins, the junctions between two olivine grains show very little deviation from the smoothly curved low-angle geometry expected for solid–melt equilibrium (Fig. 2b), whereas at the centre, extensive modification is present (e.g. Fig. 2c). There are no factors other than time that can account for this difference. The modal concentration is the same throughout the poikilocryst, and it is not possible to change the composition of the clinopyroxene (which is probably zoned, although we did not examine this) sufficiently to significantly alter interfacial energies. Hence we are forced to the conclusion that the differences reflect a variation in the period of time available to change the dihedral angle population from a melt-present one towards a melt-absent equilibrium state.

A similar conclusion must be reached for the clinopyroxene poikilocrysts in the allivalites. In these, the rounded nature of the enclosed plagioclase grains contrasts strongly with the euhedral plagioclase grains at the poikilocryst margins. This clear variation in the extent of textural equilibrium is also correlated with a difference in the dihedral angle population, with higher values in the more equilibrated central region compared with the margins.

The change in the shape and position of the frequency plot for the olivine–olivine–clinopyroxene angles (Fig. 14) must then reflect snapshots in a continuous process of changing dihedral angle, which occurred on a time-scale commensurate with that of growth of the poikilocryst. If this is correct, then the path of the dihedral angle population in the transition from a melt-bearing equilibrium towards solid-state equilibrium is different from that of a transition from a melt-bearing impingement texture towards solid-state equilibrium. The latter involves a straight trend on the median versus standard deviation plot (Fig. 1, and black dots in Fig. 10), whereas the former involves an initial steep increase in standard deviation from the melt-bearing equilibrium distribution with little corresponding increase in median angle (Figs 1 and 13). The median angle then increases with little change in standard deviation until the solid-state equilibrium is closely approached.

A further, larger scale, example is provided by analysis of a suite of allivalite samples collected at progressively greater distances below a late intrusive body of picrite (now solidified to peridotite). Holness (2005) showed that the median angle in these rocks increases from ~90° to 104° with proximity to the contact with the heat source, consistent with a low initial dihedral angle population that attained various stages in the approach to solid-state textural equilibrium.

Pertinent to a discussion of the rates of textural equilibration is the question of why we see such a fundamental difference in the topology of the interstitial melt in the peridotites compared with the allivalites. The most likely explanation is simply that olivine surfaces equilibrate more rapidly with melt than do plagioclase surfaces. Given the greater complexity of the plagioclase crystal structure, and the necessity for coupled diffusion of Ca–Al:Na–Si, this is plausible, although we are not aware of any published experimental studies comparing the two. The difference may also be controlled by the extent of supercooling during crystallization. If the melt is significantly more supercooled during the growth of plagioclase, then crystal growth will be rapid, with a consequent development of impingement textures.

That the difference in pore topology is probably a universal feature of basaltic systems is shown by the Icelandic enclaves. The olivine aggregates in these lavas (and also in the Rum parental picrite, M9) are in textural

equilibrium with the host liquid, at least on the scale of the pore corners (Fig. 5b). In contrast, the plagioclase-bearing enclaves show no signs of textural equilibration with the interstitial liquid, with impingement textures, and simple infilling of the impingement-controlled porosity by interstitial clinopyroxene (Fig. 11a).

Why do the Kameni plagioclase frameworks show significant quench-related modification of two-grain junctions whereas the Icelandic ones do not? We suggest this is the result of a fundamental difference in the two magma chamber systems. The volcanism at Santorini forms long-lived chambers dominated by cooling and fractionation, whereas that in Iceland forms hot, short-lived, chambers. It is much more likely that a significant thermal difference could develop between replenishing magma and the contents of the replenished chamber at Santorini, compared with Iceland.

There is little published work on the rates of textural equilibration, in either melt-bearing or solid systems, but an idea of the rates of sub-solidus textural equilibration can be obtained from plausible cooling and crystallization rates for magma chambers. Layers in the Rum chamber are typically of the order of 1–10 m thick, with thermal time constants of 1–100 days, suggesting that changes of dihedral angle in the sub-solidus can occur on this timescale. This is of the same order as the 4–15 days found by Holness *et al.* (1991) for attainment of equilibrium angles in calcite–olivine aggregates, and suggests that the timescale for growth of the 1 cm scale clinopyroxene poikilocrysts in the Rum allivalites is of the order of days or weeks.

The variation in dihedral angle between regions outside the clinopyroxene poikilocrysts and regions within the poikilocrysts preserves information about the solidification process in the allivalitic cumulates. If the solidification front were an infinitely thin plane the clinopyroxene should all form simultaneously as the solidification front passed upwards through the mush (assuming a simple ternary eutectic system). This would result in a constant dihedral angle within any one thin-section sized allivalite sample. However, the variation in dihedral angle across poikilocrysts, together with the fact that the foliation, defined by alignment of plagioclase laths, wraps around the poikilocrysts, shows that the growth of the poikilocrysts occurred significantly before compaction and final solidification of the mush. Clinopyroxene thus grew during a time interval, which translates to a depth interval within the mush, demonstrating that the solidification front had a finite thickness. This finite thickness is controlled perhaps by kinetic constraints of nucleation, with poikilocrysts the result of inhibition of clinopyroxene nucleation. Growth of further, interstitial, clinopyroxene and complete solidification of the mush would then occur once the mush was sufficiently supercooled to overcome the nucleation barriers.

CONCLUSIONS

A close examination of dihedral angles in natural samples demonstrates that the idea of two possible end-member textures in melt-bearing rocks is correct. Systems in which crystal growth dominates have a pore structure controlled by the impingement of growing grains. For randomly oriented crystals of plagioclase, amphibole and clinopyroxene this results in a population of angles at two-grain junctions with a median of about 60° and a standard deviation of about 25°. Such an angle population is associated with growth-controlled crystal shapes and flat interfaces at two-grain junctions. For systems in which textural equilibration dominates, the angles at two-grain junctions are much lower, with a median of 27–28° and a standard deviation of about 14°. These values are in agreement with experimentally determined dihedral angles for melt-bearing systems containing feldspar (Laporte *et al.*, 1997), amphibole (Laporte & Watson, 1995) and olivine (e.g. Bulau, 1982; von Bargen & Waff, 1988), and are associated with more rounded crystal shapes and the presence of at least some curved interfaces at two-grain junctions. Consideration of crystal shape can be used to distinguish systems in which a period of rapid, diffusion-limited, crystallization resulted in modification of two-grain junctions. Although quench growth can reduce the angle at two-grain junctions, producing angle populations indistinguishable from those produced by textural equilibration, the crystals will have elongate protuberances indicative of diffusion-limited growth (e.g. Laporte & Watson, 1995). Examination of dihedral angles in suites of completely solidified cumulates can be used to determine whether the residual porosity in the solidifying mush was dominated by grain growth or textural equilibration.

The work presented here demonstrates that equilibration of textures with disequilibrium dihedral angle populations occurs as a continuous process, with a gradual movement of the entire population towards the equilibrium final state. If the initial, pseudomorphed state is one of disequilibrium (i.e. a melt-present impingement texture) this change is accompanied by a reduction in the spread of the population. If it is one of equilibrium, the change is accompanied by an initial increase in the spread of the population, followed by a decrease. Our results provide an opportunity to constrain the timescales of magmatic processes. Essential to the progress of this novel approach is the determination of rate laws for textural change.

ACKNOWLEDGEMENTS

We are grateful to Steve Laurie for facilitating access to the Harker Collection, and to Henry Emeleus and Joseph Barraud for the loan of samples. The helpful and insightful comments of E. W. Sawyer, D. Jerram and an

anonymous reviewer greatly improved an earlier version of the manuscript. This research was funded in part by the European Community's Human Potential Programme under contract HPRN-CT-2002-000211 [EUROMELT].

SUPPLEMENTARY DATA

Supplementary data for this paper are available on *Journal of Petrology* online.

REFERENCES

Barnes, S. J. & Maier, W. D. (2002). Platinum-group elements and microstructures of normal Merensky Reef from Impala Platinum Mines, Bushveld Complex. *Journal of Petrology* **43**, 103–128.

Brenan, J. M. (1993). Diffusion of chlorine in fluid-bearing quartzite: effects of fluid composition and total porosity. *Contributions to Mineralogy and Petrology* **115**, 215–224.

Bulau, J. R. (1982). Intergranular fluid distribution in olivine–liquid basalt systems. Ph.D. thesis, Yale University, New Haven, CT, 105 pp.

Cahn, J. W. & Handwerker, C. A. (1993). Equilibrium geometries of anisotropic surfaces and interfaces. *Materials Science and Engineering* **A162**, 83–95.

Cahn, J. W. & Hoffman, D. W. (1974). A vector thermodynamics for anisotropic surfaces, II. Application to curved surfaces. *Acta Metallurgica* **22**, 1205–1214.

Campbell, I. M. (1978). Some problems with the cumulus theory. *Lithos* **11**, 311–323.

Cheadle, M. J., Elliott, M. T. & McKenzie, D. (2004). The percolation threshold and permeability of crystallising igneous rocks: the importance of textural equilibrium. *Geology* **32**, 757–760.

Cmíral, M., Fitz Gerald, J. D., Faul, U. H. & Green, D. H. (1998). A close look at dihedral angles and melt geometry in olivine–basalt aggregates; a TEM study. *Contributions to Mineralogy and Petrology* **130**, 336–345.

Didymus, J. M., Oliver, P., Mann, S., DeVries, A. L., Hauschka, P. V. & Westbroek, P. (1993). Influence of low-molecular-weight and macromolecular organic additives on the morphology of calcium carbonate. *Journal of the Chemical Society—Faraday Transactions* **89**, 2891–2900.

Donaldson, C. H. (1976). An experimental investigation of olivine morphology. *Contributions to Mineralogy and Petrology* **57**, 187–213.

Elliott, M. T., Cheadle, M. J. & Jerram, D. A. (1997). On the identification of textural equilibrium in rocks using dihedral angle measurements. *Geology* **25**, 355–358.

Emeleus, C. H. (1997). Geology of Rum and the adjacent islands. *Memoir of the British Geological Survey*, Sheet 60 (Scotland).

Faul, U. H. (1997). Permeability of partially molten upper mantle rocks from experiments and percolation theory. *Journal of Geophysical Research* **102**, 10299–10311.

Faure, F., Trolliard, G., Nicollet, C. & Montel, J.-M. (2003). A developmental model of olivine morphology as a function of the cooling rate and the degree of undercooling. *Contributions to Mineralogy and Petrology* **145**, 251–263.

Harker, D. & Parker, E. R. (1945). Grain shape and grain growth. *Transactions of the American Society of Metals* **34**, 156–195.

Harte, B., Pattison, D. R. M. & Linklater, C. M. (1991). Field relations and petrography of partially melted pelitic and semi-pelitic rocks. In: Voll, G., Töpel, J., Pattison, D. R. M. & Seifert, F. (eds) *Equilibrium and Kinetics in Contact Metamorphism: the Ballachulish Igneous Complex and its Aureole*. Heidelberg: Springer, pp. 181–210.

Herring, C. (1951*a*). Some theorems on the free energies of crystal surfaces. *Physical Review* **82**, 87–93.

Herring, C. (1951*b*). Surface tension as a motivation for sintering. In: Kingston, W. E. (ed.) *Physics of Powder Metallurgy*. New York: McGraw–Hill, pp. 143–179.

Hoffman, D. W. & Cahn, J. W. (1972). A vector thermodynamics for anisotropic surfaces, I. Fundamentals and applications to plane surface junctions. *Surface Science* **31**, 368–388.

Holness, M. B. (2005). Spatial constraints on magma chamber replenishment events from textural observations of cumulates: the Rum Layered Intrusion, Scotland. *Journal of Petrology* **46**, 1585–1601.

Holness, M. B. & Clemens, J. D. (1999). Partial melting of the Appin Quartzite driven by fracture-controlled H_2O infiltration in the aureole of the Ballachulish Igneous Complex, Scottish Highlands. *Contributions to Mineralogy and Petrology* **136**, 154–168.

Holness, M. B. & Watt, G. R. (2001). Quartz recrystallisation and fluid flow during contact metamorphism: a cathodoluminescence study. *Geofluids* **1,** 215–228.

Holness, M. B., Bickle, M. J. & Graham, C. M. (1991). On the kinetics of textural equilibration in forsterite marbles. *Contributions to Mineralogy and Petrology* **108**, 356–367.

Hunter, R. H. (1987). Textural equilibrium in layered igneous rocks. In: Parsons, I. (ed.) *Origins of Igneous Layering*. Dordrecht: D. Reidel, pp. 473–503.

Hunter, R. H. (1996). Texture development in cumulate rocks. In: Cawthorn, R. G. (ed.) *Layered Intrusions. Developments in Petrology* **15**, 77–101.

Irvine, T. N. (1987). Layering and related structures in the Duke Island and Skaergaard Intrusions: similarities, differences and origins. In: Parsons, I. (ed.) *Origins of Igneous Layering*. Dordrecht: D. Reidel, pp. 185–246.

Jamtveit, B. & Andersen, T. B. (1992). Morphological instabilities during rapid growth of metamorphic garnets. *Physics and Chemistry of Minerals* **19**, 176–184.

Jurewicz, S. R. & Jurewicz, A. J. G. (1986). Distribution of apparent angles on random sections, with emphasis on dihedral angle measurements. *Journal of Geophysical Research* **91**, 9277–9282.

Kretz, R. (1966). Interpretation of the shape of mineral grains in metamorphic rocks. *Journal of Petrology* **7**, 68–94.

Laporte, D. (1994). Wetting behaviour of partial melts during crustal anatexis: the distribution of hydrous silicic melts in polycrystalline aggregates of quartz. *Contributions to Mineralogy and Petrology* **116**, 486–499.

Laporte, D. & Provost, A. (2000). Equilibrium geometry of a fluid phase in a polycrystalline aggregate with anisotropic surface energies: dry grain boundaries. *Journal of Geophysical Research* **105**, 25937–25953.

Laporte, D. & Watson, E. B. (1995). Experimental and theoretical constraints on melt distribution in crustal sources: the effect of crystalline anisotropy on melt interconnectivity. *Chemical Geology* **124**, 161–184.

Laporte, D., Rapaille, C. & Provost, A. (1997). Wetting angles, equilibrium melt geometry, and the permeability threshold of partially molten crustal protoliths. In: Bouchez, J.-L., Hutton, D. H. & Stephens, W. E. (eds) *Granite: from Segregation of Melt to Emplacement Fabrics*. Norwell, MA: Kluwer Academic, pp. 31–54.

Longhi, J. & Jurewicz, S. R. (1995). Plagioclase–melt wetting angles and textures: implications for anorthosites. *Lunar and Planetary Science* **XXVI**, 859–860.

Lo Ré, C. F., Cheadle, M. J., Swapp, S. M. & Coogan, L. A. (2003). Sedimentation in magma chambers: evidence from the geochemistry, microstructure and crystallography of troctolite and gabbro

cumulates, Rum Layered Intrusion, Scotland. *EOS Transactions, American Geophysical Union* **84**(46), Fall Meeting Supplement, V12A-0558.

Lupulescu, A. & Watson, E. B. (1999). Low melt fraction connectivity of granitic and tonalitic melts in a mafic crustal rock at 800°C and 1 GPa. *Contributions to Mineralogy and Petrology* **134**, 202–216.

Maaløe, S. (1987). The origin of rhythmic layering. *Mineralogical Magazine* **42**, 337–345.

Maclennan, J., McKenzie, D., Gronvold, K., Shimizu, N., Eiler, J. M. & Kitchen, N. (2003). Melt mixing and crystallisation under Theistareykir, northeast Iceland. *Geochemistry, Geophysics, Geosystems* **11**, 8624, doi:10.1029/2003GC000558.

Martin, V. M., Holness, M. B. & Pyle, D. M. (2003). Windows into an open-system magma chamber: textural analysis of cognate xenoliths from the Kameni Islands, Santorini, Greece. *EOS Transactions, American Geophysical Union* **84**(46), Fall Meeting Supplement, V12A-0549.

Maumus, J., Laporte, D. & Schiano, P. (2004). Dihedral angle measurements and infiltration property of SiO_2-rich melts in mantle peridotite assemblages. *Contributions to Mineralogy and Petrology* **148**, 1–12.

McBirney, A. R. & Hunter, R. H. (1995). The cumulate paradigm reconsidered. *Journal of Geology* **103**, 114–122.

McClurg, J. E. (1982). Petrology and evolution of the northern part of the Rhum Ultrabasic Complex. Ph.D. thesis, University of Edinburgh.

Minarik, W. G. & Watson, E. B. (1995). Interconnectivity of carbonate melt at low melt fraction. *Earth and Planetary Science Letters* **133**, 423–437.

Mullins, W. W. (1957). Theory of thermal grooving. *Journal of Applied Physics* **28**, 333–339.

Mullins, W. W. (1994). Mass transport at interfaces in single component systems. *Metallurgical and Materials Transactions* **26A**, 1917–1929.

Pattison, D. R. M. & Harte, B. (1991). Petrography and mineral chemistry of pelites. In: Voll, G., Topel, J., Pattison, D. R. M. & Seifert, F. (eds) *Equilibrium and Kinetics in Contact Metamorphism: the Ballachulish Igneous Complex and its Aureole*. Heidelberg: Springer, pp. 135–180.

Platten, I. M. (1981). Partial melting of feldspathic quartzite around late Caledonian minor intrusions in Appin, Scotland. *Geological Magazine* **119**, 413–419.

Richardson-Bunbury, J. M. (1996). The Kula Volcanic Field, Western Turkey: the development of a Holocene alkali basalt province and the adjacent normal faulting graben. *Geological Magazine* **133**, 275–283.

Riegger, O. K. & Van Vlack, L. H. W. (1960). Dihedral angle measurement. *Transactions of the Metallurgical Society of the AIME* **218**, 933–935.

Rosenberg, C. L. & Riller, U. (2000). Partial melt topology in statically and dynamically recrystallised granite. *Geology* **28**, 7–10.

Sachenko, P. P., Schneibel, J. H. & Zhang, W. (2004). Observations of secondary oscillations in thermal grain boundary grooves. *Scripta Materialia* **50**, 1253–1257.

Sawyer, E. W. (1999). Criteria for the recognition of partial melting. *Physics and Chemistry of the Earth* **24**, 269–279.

Sawyer, E. W. (2001). Melt segregation in the continental crust: distribution and movement of melt in anatectic rocks. *Journal of Metamorphic Geology* **19**, 291–309.

Smith, C. S. (1948). Grains, phases and interfaces: an interpretation of microstructure. *Transactions of the Metallurgical Society of the AIME* **175**, 15–51.

Swanson, S. E. & Fenn, P. M. (1986). Quartz crystallisation in igneous rocks. *American Mineralogist* **71**, 331–342.

Tepley, F. J., III & Davidson, J. P. (2003). Mineral-scale Sr-isotope constraints on magma evolution and chamber dynamics in the Rum layered intrusion, Scotland. *Contributions to Mineralogy and Petrology* **145**, 628–641.

Tiller, W. A. (1991). *The Science of Crystallisation: Macroscopic Phenomena and Defect Generation*. Cambridge: Cambridge University Press, 484 pp.

Toramaru, A. & Fujii, N. (1986). Connectivity of the melt phase in a partially molten peridotite. *Journal of Geophysical Research* **91**, 9239–9252.

Upton, B. G. J., Skovgaard, A. C., McClurg, J., Kirstein, L., Cheadle, M., Emeleus, C. H., Wadsworth, W. J. & Fallick, A. E. (2002). Picritic magmas and the Rum ultramafic complex, Scotland. *Geological Magazine* **139**, 437–452.

Vernon, R. H. (1968). Microstructures of high-grade metamorphic rocks at Broken Hill, Australia. *Journal of Petrology* **9**, 1–22.

Vernon, R. H. (1970). Comparative grain-boundary studies of some basic and ultrabasic granulites, nodules and cumulates. *Scottish Journal of Geology* **6**, 337–351.

Vernon, R. H. (1997). Comment: On the identification of textural disequilibrium in rocks using dihedral angle measurements. By Elliott, M. T. & Cheadle, M. J. *Geology* **25**, 1055.

von Bargen, N. & Waff, H. S. (1988). Wetting of enstatite by basaltic melt at 1350°C and 1·0–2·5 GPa pressure. *Journal of Geophysical Research* **93**, 1153–1158.

Waff, H. S. & Bulau, J. R. (1979). Equilibrium fluid distribution in an ultramafic partial melt under hydrostatic stress conditions. *Journal of Geophysical Research* **84**, 6109–6114.

Wager, L. R., Brown, G. M. & Wadsworth, W. J. (1960). Types of igneous cumulates. *Journal of Petrology* **1**, 73–85.

Wark, D. A., Williams, C. A., Watson, E. B. & Price, J. D. (2003). Reassessment of pore shapes in microstructurally equilibrated rocks with implications for permeability of the upper mantle. *Journal of Geophysical Research* **108**(B1), 2050, doi:10.1029/2001JB001575.

Zhang, W., Sachenko, P. & Schneibel, J. H. (2002). Kinetics of thermal grain boundary grooving for changing dihedral angles. *Journal of Materials Research* **17**, 1495–1501.